Role of the Renner-Teller effect after core hole excitation in the dissociation dynamics of carbon dioxide dication

J. Laksman, E. P. Månsson, C. Grunewald, A. Sankari, M. Gisselbrecht, D. Céolin, and S. L. Sorensen

Citation: The Journal of Chemical Physics **136**, 104303 (2012); doi: 10.1063/1.3692293
View online: http://dx.doi.org/10.1063/1.3692293
View Table of Contents: http://scitation.aip.org/content/aip/journal/jcp/136/10?ver=pdfcov
Published by the AIP Publishing

Role of the Renner-Teller effect after core hole excitation in the dissociation dynamics of carbon dioxide dication

J. Laksman,[1,a)] E. P. Månsson,[1] C. Grunewald,[2] A. Sankari,[1] M. Gisselbrecht,[1] D. Céolin,[1,3] and S. L. Sorensen[1]
[1]*Department of Synchrotron Radiation Research, Lund University, S-221 00 Lund, Sweden*
[2]*Institute of Chemistry and Biochemistry, Freie Universität Berlin, Takustraße 3, 14195 Berlin, Germany*
[3]*Synchrotron SOLEIL, L'Orme des Merisiers, St. Aubin BP 48, F-91192 Gif-Sur-Yvette, France*

(Received 25 November 2011; accepted 17 February 2012; published online 9 March 2012)

The fragmentation of the doubly-charged carbon dioxide molecule is studied after photoexcitation to the C $1s^1 2\pi_u$ and O $1s^1 2\pi_u$ states using a multicoincidence ion-imaging technique. The bent component of the Renner-Teller split states populated in the $1s \rightarrow \pi^*$ resonant excitation at both the carbon and oxygen 1*s* ionization edges opens pathways to potential surfaces in highly bent geometries in the dication. Evidence for a complete deformation of the molecule is found in the coincident detection of C^+ and O_2^+ ions. The distinct alignment of this fragmentation channel indicates rapid deformation and subsequent fragmentation. Investigation of the complete atomization dynamics in the dication leading to asymmetric charge separation shows that the primary dissociation mechanisms, sequential, concerted, and asynchronous concerted, are correlated to specific fragment kinetic energies. The study shows that the bond angle in fragmentation can extend below 20°. © *2012 American Institute of Physics*. [http://dx.doi.org/10.1063/1.3692293]

I. INTRODUCTION

Dynamic effects in molecules have been studied for many years using spectroscopic methods but direct information about isomerization, charge transfer, and dissociation obtained using novel techniques based upon imaging of charged fragments has been a driving force in the large number of studies combining spectroscopic and geometric information.[1,2] A fundamental motivation for studying such phenomena is understanding the connection between the quantum chemical picture and photoinduced dynamics. While synchrotron radiation allows selective ionization or excitation to specific electronic states, advances in sophisticated techniques for measuring the complete momentum of ionic fragments produced after photoionization has illuminated the connection between electronic states and molecular geometries through powerful analysis tools relying on multi-particle imaging techniques.[1] These methods are particularly powerful for studies of fragmentation in dicationic or tricationic species where several ionic fragments are measured and a complete kinematic picture is obtained.[3] An important aspect is the mechanism behind molecular fragmentation and how the dynamics associated with geometric changes in the molecule are coupled to fragmentation.

Rapid geometry changes in core-excited molecules are documented in many experimental studies using synchrotron radiation for core-electron excitation.[4–9] Measurements of the molecular frame photoelectron angular distributions (MFPAD) after C 1*s* and O 1*s* ionization in carbon dioxide reveal that at the carbon 1*s* edge an asymmetry in the MFPAD is correlated with the asymmetric two-body fragmentation channel, while at the oxygen 1*s* edge the bond to the core-ionized oxygen atom is elongated in the process leading to CO^+/O^+ fragmentation.[10,11] The core-excited Π states are doubly degenerate in the linear geometry of the ground-state carbon dioxide molecule, and split into two states (in-plane and out-of plane orbitals) due to the Renner-Teller effect. In carbon dioxide the bent geometry in the core-excited states is well established, both through the equivalent-cores approximation (NO_2 is bent in the ground state) and theoretical studies and through angle-resolved ion yield measurements.[12,13] The bond angle was calculated to be 134.3° at the C $1s^1 2\pi_u$ and 127.8° at the O $1s^1 2\pi_u$ but Muramatsu *et al.*[9] separated the linear and bent components using triple-ion coincidence spectroscopy and showed that the bond angle is reduced to about 100° on the time scale of the Auger decay (6 fs for carbon 1*s*).

Carbon dioxide is a veritable showcase for understanding the complexities of photodissociation and is a classic case for illuminating symmetry-breaking effects connected with vibronic coupling. Recent work highlights dissociative processes in carbon dioxide that illustrate the effects of geometry on dissociation in core-excited states,[4,5,9,13,14] ion-yield measurements identified both anions and cations produced in photoionization,[15] and fragmentation mechanisms were studied using multi-ion coincidence methods after photoexcitation,[16–19] electron impact,[20] and ion impact ionization.[3] A number of recent studies focus on triply ionized carbon dioxide[21] and its fragmentation.[3,9,18,20,22] The latter studies rely on multi-coincidence imaging studies. Despite the fact that core-excited carbon dioxide is well studied, and has been over many years, the molecule continues to play an important role in new discoveries especially in fragmentation dynamics.

Dicationic states have been extensively studied in the valence and inner-valence regions which are the relevant states

a)Author to whom correspondence should be addressed. Electronic mail: joakim.laksman@sljus.lu.se.

for the final dissociative states populated after the decay of core-excited states. Masuoka[23] measured the vertical threshold for CO^+/O^+ at 39.2 ± 0.3 eV. Hochlaf *et al.*[24] calculated potential energy surfaces along the CO bond coordinate. In particular, they found that the dication ground state $CO_2^{2+}(X^3\,\Sigma_g^-)$ has a significantly smaller dissociation barrier than other low-lying states. Correlation of this potential energy surface to the $CO^+(X^2\Sigma)/O^+(^4S_0)$ fragmentation channel with a kinetic energy release (KER) of 6 eV was found in several studies using different approaches.[19,25,26] The anisotropy of ejected fragments in CO_2 has been studied in this energy range where Masuoka[16] and Alagia *et al.*[25] reported anisotropic ion distributions for the primary dissociation channels. Eland *et al.*[21] measured triply ionized states populated via core-electron excitation and found the lowest states at about 70 eV.

In the present study, we measure the kinematics of dication fragmentation after photoexcitation at the carbon and oxygen 1*s* edges. Evidence for severe deformation of the molecule is found in the ion pair C^+/O_2^+ at the $1s^{-1}2\pi_u$ states for both carbon and oxygen core-electron excitation. Analysis of the three-body dissociation channel clearly shows that the fragmentation process itself is correlated to the energy of fragmentation and that sequential fragmentation where the CO bonds are broken in two steps is enhanced at the $2\pi_u$ resonances. We find that the low-energy fragmentation channels correspond to the largest bond angle change and likely evolve into the fragmentation channel which produces O_2^+.

II. EXPERIMENT

An imaging time-of-flight multi-coincidence spectrometer is used to measure the momenta of all ionic fragments using a separate electron detector as a start signal. The spectrometer is mounted with the time-of-flight axis mutually perpendicular to the polarization vector of the x rays and to the propagation direction of the synchrotron light as shown in Fig. 1(a). The spectrometer has a two-stage acceleration with an electrostatic lens for optimal ion focussing to an 80 mm diameter delay-line detector (ROENTDEK DLD80). The sample is introduced via an effusive gas jet producing a background pressure of 5×10^{-6} mbar during measurements. The radial energy scale was calibrated to the kinetic energy of the C^+/O^+ fragments from carbon monoxide at the C $1s\rightarrow 2\pi_u^*$ resonance.[27] The lens potential used in this study ensures that all ions up to a kinetic energy of about 19 eV are collected; this has been verified in separate studies.[28] The measurements were performed at the soft x ray undulator beamline I411 at MAX-lab in Lund, Sweden.[29] The contribution from second-order light for the photon energies in this study is negligible.

The raw data for each event are transformed into a three-dimensional momentum space and subsets of the data are extracted by filtering by angular criteria, momentum or according to dissociation channel. In the case where the axial-recoil approximation is valid and the molecular rotation can be ignored, the anisotropy of the fragment ions is directly related to the angle between the dipole moment and the fragment ejection.[30] This is especially true for ionic fragments ejected with higher kinetic energy.[31] The kinematics are extracted directly from the momentum data, and the molecular anisotropy parameter, β, can be determined for any subset of data filtered by ion mass, kinetic energy or angular considerations.

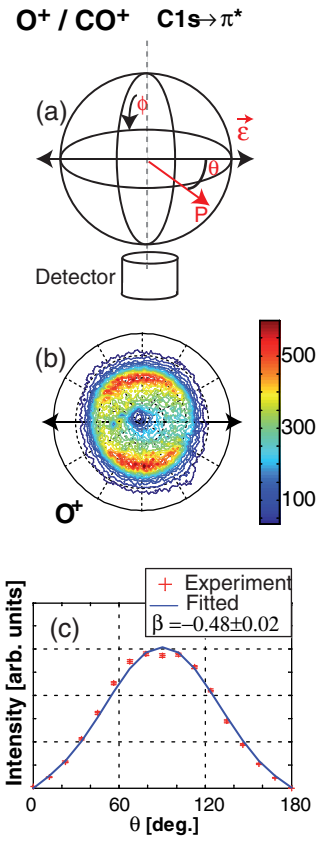

FIG. 1. (a) Schematic diagram of the geometry of the setup. $\vec{\epsilon}$ is perpendicular to the propagation direction of the synchrotron radiation and to the spectrometer axis (vertical). P is the momentum vector of an ion. (b) Detector image of O^+ measured in coincidence with CO^+ at the C $1s\rightarrow \pi^*$ resonance. The arrow indicates the direction of the polarization vector. (c) The distribution of measured ions as a function of angle θ is shown including statistical error bars. Each point represents the integration over $\phi = 0 \rightarrow \pi$, and over $\Delta\theta = 11.25°$. The solid line shows the best fit of Eq. (4). The best fit was found for $\beta = -0.48 \pm 0.02$.

The conventional expression for the differential cross section is

$$\frac{d\sigma}{d\Omega} = \frac{\sigma}{4\pi}[1 + \beta P_2(\cos\theta)], \tag{1}$$

where σ is the total cross section integrated over space and P_2 is the second-order Legendre polynomial, $P_2(x) = (3x^2 - 1)/2$. The geometry of our setup is shown in Fig. 1(a). Since the fragment intensity is symmetric about the polarization vector the angular distribution of fragments can be expressed as[32]

$$I(\theta) = \frac{\sigma}{4\pi}\int [1 + \beta P_2(\cos\theta)]d\Omega, \tag{2}$$

where $d\Omega = \sin\theta d\theta d\phi$ and ϕ is the azimuthal angle, so

$$I(\theta) = \frac{\sigma}{4\pi}\int_0^{2\pi} d\phi \int_\theta^{\theta+\delta\theta} d\theta \sin\theta[1 + \beta P_2(\cos\theta)] \tag{3}$$

with the solution for the case where $\delta\theta \rightarrow 0$

$$I(\theta) = \frac{\sigma}{2}\sin\theta[1 + \beta P_2(\cos\theta)]. \tag{4}$$

Sources of systematic error in the determination of β include nonuniform detector efficiency, errors in the spatial, and temporal coordinates as well as the direction of the polarization vector, $\vec{\epsilon}$. In order to estimate the sensitivity of the β value to these errors, we translated the (T,X,Y) coordinates raw data by 3.0 ns in time and $\pm$2.0 mm on the detector and rotated $\vec{\epsilon}$ by 3°. For double coincidences of two-body breakups, θ is taken as the mean value for the two particles. We confirmed that the histogram bin size has no effect on the determination of the β parameter. For channels with good statistics, this led to an error estimate $\sim\pm0.03$ for β.

An illustrative example is the O^+/CO^+ two-body dissociation channel at the C $1s\rightarrow 2\pi_u^*$ resonance. The angular distribution of the O^+ fragment from this pair about the time-of-flight axis is shown in Fig. 1(b). The radial plot shows a distribution characteristic of a perpendicular alignment of the molecule with respect to the polarization vector as expected for a $\Sigma - \Pi$ dipole excitation. In Fig. 1(c), the experimental data are presented as a function of angle together with a fit to Eq. (4). The best fit is found for a β value -0.48 ± 0.03. While the corresponding bond angle is in accord with the 135° bond angle expected from the equivalent-cores model, Bozek *et al.*[17] measured value for the O^+ fragment was somewhat smaller presumably due to contributions from other fragmentation channels producing the same fragment. Our measured asymmetry parameter for the O^+/CO^+ fragmentation channel corresponds very well to the 134.3° bond angle for the C $1s\rightarrow 2\pi_u^*$ resonance calculated by Ehara and Ueda.[12]

III. RESULTS AND DISCUSSION

The core-valence excited states in carbon dioxide are well known to exhibit dynamic effects. The excitation of the O 1*s* or C 1*s* electrons to the unoccupied $2\pi_u$ orbital lift the degeneracy of the lower bent (A_1), and the higher linear (B_1) state by the Renner-Teller effect.[6] Symmetry-resolved studies focusing on the angular properties of ion yield reveal the importance of vibronic coupling[13,33,34] and ion momentum imaging studies of the fragments from triply ionized CO_2 confirm the geometric differences for the Renner-Teller split A_1 and B_1 states.[9] At the low-energy side of the $2\pi_u^*$ resonance the bent state is preferentially populated. We expect that these states will decay via Auger processes to areas of the potential energy surface where the bond angle is substantially less than 160°.[9] In Muramatsu's study, the distribution of bond angles measured in triple-ion coincidences clearly shows that the A_1 state is associated with smaller bond angles (down to about 90°) while the linear B_1 state has a distribution peaking at 160° but extends to about 130°. The large deformation in the C $1s\rightarrow 2\pi_u^*$ resonance can open decay channels to potential surfaces in the dication where the bond angle is small. A signature can be found in the two-body breakup leading to the dissociation limit C^+/O_2^+ highlighting a precursor bent geometry. A first outcome is the complete deformation of the molecule, leading to a transient isomerization, and the subsequent dissociation where both C–O bonds are broken and the oxygen atoms bond together.

A. Transient isomerization

We investigate the transient isomerization channel by looking at the ion pair C^+/O_2^+ at both the C $1s\rightarrow 2\pi_u^*$ resonance and at the O $1s\rightarrow 2\pi_u^*$ resonance. In Fig. 2(a), we show a polar plot of all C^+ ions measured in coincidence with O_2^+ at the C $1s\rightarrow 2\pi_u^*$ resonance. The distribution of fragments indicates a preference along the polarization direction. In Fig. 2(b), the angular distribution of C^+ ions from this pair is presented for the C 1*s* and O 1*s* resonances together with a least-squares fit of Eq. (4). The fits produce values of $\beta = 1.07\pm0.14$ at the C 1*s* edge and 0.78 ± 0.15 at the oxygen edge. The strong anisotropy of the angular distribution indicates that the C–O bond break takes place along the direction of the polarization vector. Interestingly, the case shown in Fig. 1(b) for a single O^+ ejection reveals that the molecular orientation in the excited state is perpendicular to this direction. The measured distribution of C^+ and O_2^+ pairs is thus evidence of a dramatic geometry change, but the initial perpendicular alignment of the nearly linear molecule evolves to an alignment of the molecule parallel to the polarization

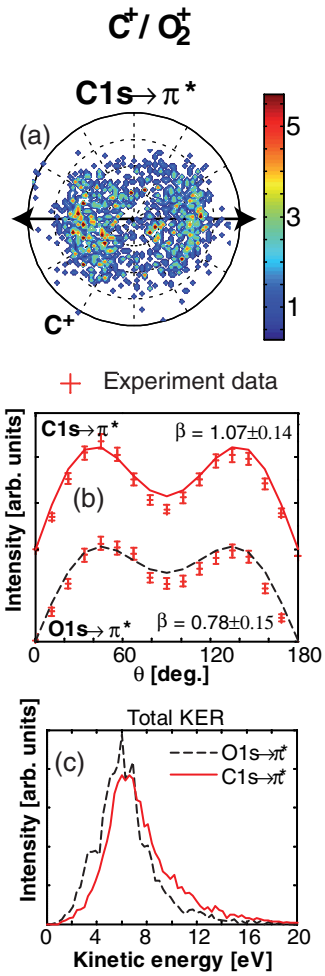

FIG. 2. (a) Distribution of C^+ ions measured in the C^+/O_2^+ coincidence events at the C $1s\rightarrow \pi^*$ resonance. The arrow indicates the direction of the polarization vector. (b) The distribution of ions as a function of angle θ as in Fig. 1. The lines shows the best fits of Eq. (4). (c) The distribution of total kinetic energy of the fragment pair is shown for excitation at C $1s\rightarrow \pi^*$ and O $1s\rightarrow \pi^*$.

direction as a consequence of deformation. The sharpness of the distribution reflects the rapidity of the dissociation with respect to the rotational period. We infer that deformation occurs during the bending motion, and that both deformation and dissociation are prompt on the time scale of rotation. At the O $1s\rightarrow \pi^*$ resonance the measured anisotropy is less sharp ($\beta = 0.78$), which indicates an asymmetric intermediate state where the dipole moment is shifted from the bisector as predicted by Ehara's theoretical study.[12]

The KER distributions provide additional information relevant to the fragmentation process. The KER in two-body dissociation channels reflects the vertical distance the wave packet moves on the potential surface in the dication as it dissociates. In Fig. 2(c), we present the KER distribution for the O_2^+/C^+ channel. This peak is rather narrow with a maximum at ~7 eV suggesting that this pair can break into only a few final states and pathways. With no internal electronic energy in the fragments, the adiabatic dissociation limit is ~6.5 eV lower than the adiabatic dissociation limit for the complete atomization $C^+/O^+/O$, suggesting that competition between these two channels can occur if the nuclear wave packet is outside the Franck Condon region after electronic relaxation. The distribution for the O 1*s* resonance is similar.

The enhancement of the bending motion in these core-excited states allows the possibility of decay to severely transient bent states that are not accessible in the linear geometry or for small bond angles. Öhrwall *et al.*[15] reported detection of the O_2^+ fragment in a partial ion yield study at the oxygen and carbon 1*s* ionization edges. They also found a very low intensity except at the resonances of interest in this study and at the first Rydberg state in the C 1*s* absorption spectrum. Although this dissociation channel is relatively weak, we have evidence that the strongly deformed molecular geometry is only accessible through the dicationic state since O_2^+ is only detected in coincidence with C^+ despite the higher efficiency of the single-ion coincidence measurement. We believe that the fragment they detected arose from the dication fragmentation. Both Öhrwall's partial ion yield and our measurements confirm that at the O $1s\rightarrow \pi^*$ resonance the branching ratio for this pathway is about half of that found at the C 1*s* edge. Assuming a constant decay rate from the core-excited state to the dication leading to this fragmentation channel, it becomes evident that the branching ratio between the O $1s\rightarrow \pi^*$ and C $1s\rightarrow \pi^*$ should be proportional to the ratio of the core-hole lifetimes (3.5 fs and 6 fs) which is approximately 0.5.

There are no calculations available in the literature which describe this highly deformed dissociation channel in CO_2. Experimental evidence for similar effects in other linear molecules can provide a model for the nuclear dynamics. A fragmentation channel indicating a dibridged configuration was identified in acetylene.[35] This channel was isolated by filtering on H_2^+/C_2^+ coincidences and it was found that we monitor only molecules undergoing a *cis*-bending motion. The sharp alignment that was registered for acetylene in the C $1s^{-1}\pi^*$ state ($\beta = 1.1$) could be rationalized due to the small inertia of the terminal hydrogen fragments. Our previous study of carbonyl sulphide found a similar phenomenon leading to C^+/OS^+ with a less pronounced anisotropy parameter interpreted as a signature of a significantly longer time scale for this transient isomerization.[36] The rearrangement in CO_2 can be seen as an intermediate case. Despite the larger inertia of oxygen, our analysis arrives at the same value of the anisotropy parameter as for acetylene. A plausible explanation is that core electron excitation to the Renner-Teller split C/O $1s^{-1}2\pi_u$ state in carbon dioxide leads to highly bent molecules, and the oxygen lone-pair orbitals are strongly attractive and the oxygen atom and ion can bond relatively quickly.

B. Asymmetric charge separation: Dissociation mechanisms and fragment energy correlations

A second outcome of the Renner-Teller effect in the core excited states is to influence dissociation dynamics in other channels. In line with Muramatsu's study[9] indicating an angular distribution with a peak at 100° for the highest dissociation limit (triply ionized), we investigate the dissociation limit leading to an asymmetric charge-separation channel with neutral evaporation from the dication. The threshold for the $C^+/O^+/O$ channel is at 47.2 ± 0.5 eV (Ref. 26) and the mean kinetic energy of the two detected fragments is found to have a maximum of 7 eV over the 60–100 eV photon energy range.

We carried out measurements in this energy range and at several energies near the C and O $1s\rightarrow \pi^*$ resonances. We detect O^+ and C^+ in coincidence and the energy of the undetected oxygen fragment is deduced via conservation laws. The undetected fragment could in principle be either a neutral oxygen atom or an oxygen ion, although for energies below the triple ionization threshold at about 70 eV the third fragment must be neutral. Both the fragment KE distribution and the total KER distribution of the reaction are observables which can distinguish different dissociation mechanisms.[3,16] Our study reveals kinematics similar to studies at higher energies where a detailed analysis of the mechanism based on Newton diagrams assuming a dication mother species was performed.[20,37]

The Dalitz plot is a valuable tool for analyzing the kinematics of the fragments and their correlations. The energy correlation between fragments directly reflects the fragmentation mechanism and the dynamics involved in dissociation. The normalized coordinates ϵ_i used in the Dalitz plot are defined as

$$\epsilon_i = \frac{|\vec{p}_i|^2}{\sum_{i=1}^{3} |\vec{p}_i|^2}, \tag{5}$$

and $\vec{p}_i$ is the momentum vector of fragment $i \in \{1, 2, 3\}$. The kinematic constraint, $\sum_i \epsilon_i \equiv 1$, requires that all points lie in a plane. Conservation of linear momentum $\sum_i \vec{p}_i \equiv \vec{0}$, introduces the additional constraint that all points must lie within the unit circle. Introduction of Cartesian coordinates $x_D = (\epsilon_2 - \epsilon_3)/\sqrt{3}$ and $y_D = \epsilon_1 - 1/3$ allows data to be presented in a 2D Dalitz plot from which the vector correlation between fragments can be deduced.[38,39] The case where particle *i* has zero momentum corresponds to the point on the circle where the tangent is perpendicular to the ϵ_i axis. The

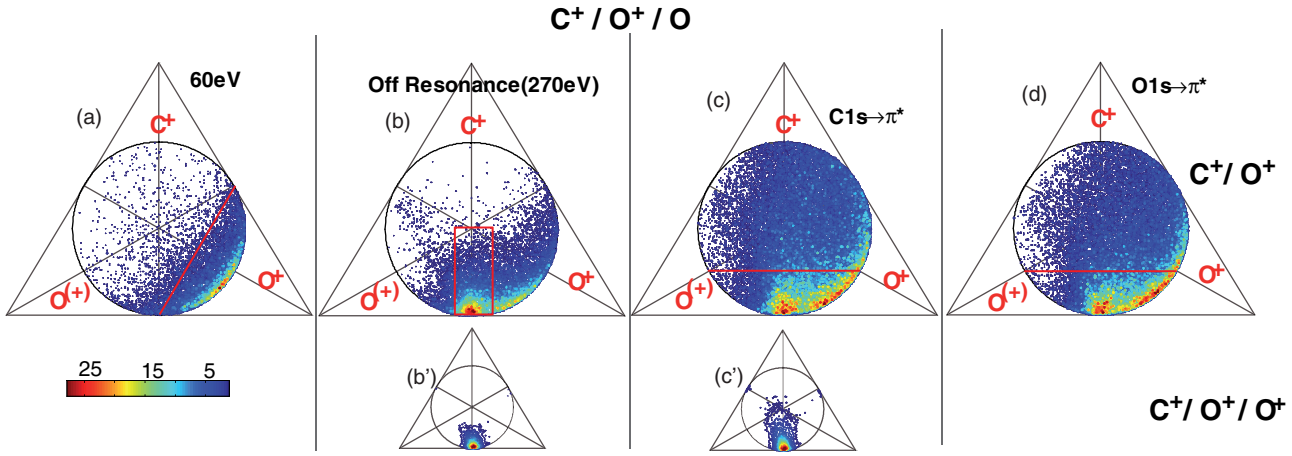

FIG. 3. Dalitz plots of the fragments measured at different photon energies for three-body fragmentation events. The upper plots are for detection of C^+ in coincidence with O^+, and the lower plots show the distribution for detection of three charged fragments. (a) Photon energy of 60 eV, (b,b′) 270 eV, (c,c′) 290.7 eV (C $1s\rightarrow \pi^*$), and (d) 535.4 eV (O $1s\rightarrow \pi^*$).

opposite point represents the maximum value, $\epsilon_i = \frac{2}{3}$. At the center of the circle all fragments have equal momenta.

For sequential dissociation in the ABC molecule (ABC→A/BC→A/B/C), the diatomic fragment, BC, has time to rotate between the first and second dissociation steps. In this case, we expect B and C to be anti-correlated, while A, which receives a nearly constant fraction of the total KER, is uncorrelated to the other fragments. For a concerted process, the geometry is nearly fixed during fragmentation and the Coulomb force determines the kinetic energies. This produces a well-defined pattern in the Dalitz plot.

Dalitz plots for $C^+/O^+/O$ at 60 eV, 270 eV, and the C/O $1s\rightarrow \pi^*$ resonances are shown in Fig. 3. We can distinguish between sequential and concerted processes in these plots.[8] In Fig. 3(a) (below and to the right of the red line). the distribution is nearly perpendicular to the O^+ axis, indicating weak correlation between the oxygen cation and all other fragments. The diagram indicates that C^+ and the neutral oxygen are strongly anti-correlated. This is characteristic of a sequential dissociation process, where the primary fragment is O^+ and the second dissociation step occurs after the charged fragments have left the Coulomb region. These mechanisms have been identified in CO_2 previously by Masuoka and by Tian via photo-electron-photo-ion-photo-ion-coincidence slope analysis.[22,26] At the higher photon energies in Fig. 3(b) (inscribed in the red rectangle), an additional feature is visible in the region where C^+ has its minimum energy partition. The symmetry of this feature along the ϵ_{C^+} axis is due to the fact that the oxygen fragments have equal kinetic energies. All of the fragments are uncorrelated, which is characteristic of a concerted process with all particles in the Coulomb region during fragmentation. This concerted process was also observed in Pešič's Newton diagrams below the O $1s^{-1}2\pi_u$ state and was associated with C^+ fragments with low kinetic energy.[37] This is commensurate with a linear geometry that fragments symmetrically.

One possible explanation for the appearance of a new fragmentation channel in Fig. 3(b) is triple ionization. It is more likely in this weak asymmetric charge separation channel ($C^+/O^+/O$) that an event producing three ionic fragments be detected as a double-coincidence event due to the finite detection efficiency and electronics dead time of about 10 ns which significantly affects the detection probability of two O^+ ions. In the spectrum measured at 270 eV, these events account for about 65% ± 5% of measured events. Our triple-ion coincidence data confirm the hypothesis indirectly since the concerted feature is essentially identical to the plot of the true $C^+/O^+/O^+$ trication fragmentation. These data are shown in Fig. 3(b′) for 270 eV. The concerted dissociation would result in a relatively large flight time difference between the two oxygen ions since the velocity vectors are nearly parallel to the spectrometer axis thus increasing the probability of detecting two oxygen ions for that particular channel. This interpretation is supported by a recent study of CO_2^{3+} produced in collisions with Ar^{8+} ions by Neumann *et al.*[3]

The Dalitz plot at the C $1s^{-1}2\pi_u$ in Fig. 3(c) state shows a different pattern. There are true coincidence events over essentially the entire plot area indicating that all fragment energy partitions are equally likely. The most striking difference from the off-resonance plot is the large number of higher-energy C^+ ions. At the O $1s^{-1}2\pi_u$ state in Fig. 3(d) we see a similar trend. In the Dalitz plots for the $C^+/O^+/O^+$ at the same resonance in Fig. 3(c′) this component is significantly weaker suggesting it to be a true feature of the dication.

High C^+ kinetic energy indicates a bent molecular geometry: The higher the kinetic energy of the central atomic ion the smaller the bond angle. Not surprisingly this feature is seen at the carbon and oxygen $1s\rightarrow 2\pi_u^*$ resonances, both known to have bent geometries, and where the C^+/O_2^+ ion pair is measured. In another study at the O $1s\rightarrow 2\pi_u^*$ resonance,[37] the *deferred charge-separation* mechanism was proposed to explain the energetics. Such a process implies strong anti-correlation between C^+ and O^+ which is not supported by the Dalitz plot in Fig. 3(d).

Neumann *et al.* found that the total energy deposited in the CO_2 molecular ion determines the fragmentation pathway.[3] The events characterized by anti-correlated C^+ and O energies can be isolated with a particular energy filter;

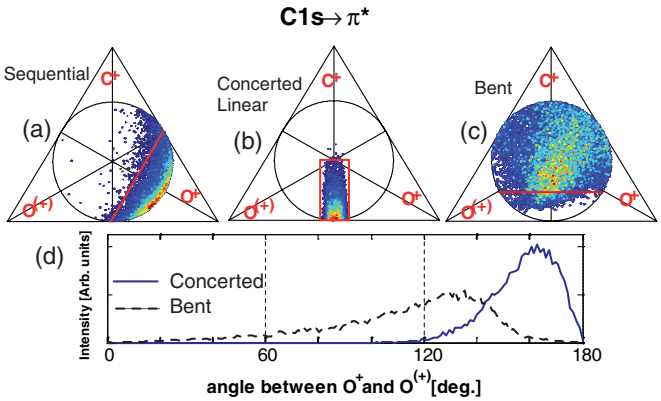

FIG. 4. Dalitz plots of kinetic-energy filtered subsets of ionic C and O fragments measured at the C 1*s*-π^* resonance. (a) Events fulfilling the criteria 1 eV $< E(C^+) + E(O) \cdot \frac{12}{16} < 5$ eV. These correspond to sequential dissociation originating in the carbon dioxide dication. (b) Coincidence events fulfilling the criteria -2 eV $< E(O^+) - E(O) < 2$ eV and 13 eV $< E(O^+) + E(O)$. These correspond to concerted breakup from the linear trication. (c) The high-energy carbon fragment (5 eV $< E(C^+)$) indicates concerted breakup from the severely bent dication. (d) Angular correlation plots for the data from the subsets in (b) and (c).

in this case 1 eV<KE(C^+) + $\frac{12}{16}$KE(O)<5 eV. The result is shown in Fig. 4(a) where Dalitz plots for filtered subsets of $C^+/O^+/O$ at the C 1*s*→ π^* resonance are shown. The concerted dissociation pathway is characterized by strong correlation between O^+ and $O^{(+)}$ as well as high fragment kinetic energies. A subset where both oxygens have large and approximately equal KER effectively selects this set of events. The -2 eV<KE(O^+) $-$KE($O^{(+)}$) < 2 eV and 13 eV<E(O^+) + E($O^{(+)}$) intervals efficiently filter out other processes [see Fig. 4(b)]. To isolate the bent component we chose events where the C^+ fragment has more than 5 eV. This data subset is shown in Fig. 4(c).

Figures 4(a)–4(c) illustrates how the energy correlation separates these three dissociation pathways. Since the data also contain angular information, the angular correlation for each event can be plotted as a histogram. The result is shown in Fig. 4(d) where two distinct cases are compared and a distinct angular signature is exhibited for each of the dissociation mechanisms in Figs. 4(b) and 4(c). The events in the concerted process subset have a peak at an $\vec{p}_{O^{(+)}}$ and $\vec{p}_{O^+}$ angle of about 160° and the distribution extends to 120°. The angular correlation of the bent component shown in Fig. 4(c) indicates a significantly smaller angle with a peak at around 130°. It is significant that the distribution of the angular correlation extends to below 20°. This result is interesting and can be interpreted as a link between the complete deformation measured in the two-body C^+/O_2^+ dissociation case.

Although these correlations are based upon one measured oxygen ion and the deduced momentum of the second oxygen atom there is reason to compare with the triple-ionization case. For the linear component the angular correlation we measure is very similar to that reported by Muramatsu, but the bent distribution is rather different.[9] While the similarity in the angles in the linear component for these measurements could be due to our finite dead time, the situation is somewhat more fortunate in the latter case. The probability of detecting all three ions is highest when the alignment of the molecule maximizes the flight-time difference between the two oxygen ions. This occurs when the molecular axis, and hence the O–H bonds, is aligned parallel to the spectrometer axis. The time difference between the detection of the two identical oxygen ions also increases with oxygen fragment energy projected along the spectrometer time-of-flight axis. In Fig. 3, we compare our ion-ion coincidence measurements at (b) 270 eV and (c) at the C 1*s*→ π^* state with true triple coincidences at the same two energies. The Dalitz plots of triple coincidences in Fig. 4 (b) and (c) contain mainly events where the carbon ion has a low kinetic energy (more linear geometry) while almost no events with higher carbon kinetic energies are measured as triple coincidences (bent geometries). The electronics dead time prohibits measurement of both oxygen ions for all such events, and the measurement is registered as a double-coincidence event instead. We conclude that for the linear geometry a large fraction of our measurement consists of two fragments from the trication breakup (i.e., aborted triple coincidences), resulting in an angular distribution very similar to Ref. 9. For the bent case, we find a distribution which differs significantly from the triply ionized case, and is truly a dication fragmentation event.

As the dication dissociates into three fragments the lone-pair orbitals in the oxygen ion and atom lead to a probable bonding of these two fragments, rather than a repulsion of positive ions as was seen in the trication dissociation. Our result shows that a significant fraction of molecules have a geometry with an angle less than 90°. Since there is no visible cutoff angle (as is the case for triple ionization), we believe that the existence of the O_2^+ fragment is a natural consequence of the large bending angle in the A_1 state at the C 1*s*→ π^* resonance. Analysis of our double- and triple-coincidence data at the O 1*s*→ π^* state shows a similar pattern although the average angles are slightly larger.

This study demonstrates that while angle-resolved ion yield measurements provide an average picture of the alignment and geometry, fully coincident measurements of fragment 3D momenta reveals the details of individual dissociation channels, which essentially brings the measurement close to the molecular frame. In carbon dioxide, we see that the main dissociation channel O^+/CO^+ is commensurate with a bond angle of about 135° at the C 1*s*→ π^* resonance, while the O^+/C^+ fragmentation channel is associated with a broad range of angles ranging from linear to a highly bent geometry. The third channel, O_2^+/C^+ provides insight into the complete deformation of the molecule which though relatively weak, is easily isolated in these measurements.

IV. CONCLUSION

We investigated the fragmentation of the carbon dioxide dication after core-excitation to the C and O $1s^{-1}2\pi_u$ states. Two-body dissociation into O^+/CO^+ results in identical KER distributions that are independent of photon energy. The ground state of the dication is populated with a high probability in electronic transitions leading to this fragmentation channel. We show that the bending vibrational mode induced after core-excitation to the C $1s^{-1}2\pi_u$ state can decay into a

dication state that subsequently dissociates into the C^+/O_2^+ pair. Three-body breakup of the dication into $O^+/C^+/O$ is mainly a sequential two-step process. At the low-energy side of the C/O $1s \rightarrow \pi^*$ resonance we find evidence of a Coulomb explosion channel induced by the bent Renner-Teller component. Energy correlations of the fragments are studied using Dalitz plots. The energy correlations provide a tool to select events corresponding to particular dissociation mechanisms which can be analyzed for angular information.

ACKNOWLEDGMENTS

We gratefully acknowledge assistance from the MAX-lab staff, in particular to Maxim Tchaplyguine. Funding for this work was granted from the Knut and Alice Wallenberg Foundation and the Swedish Research Council (VR). A. S. acknowledges also the Research Council for Natural Sciences and Engineering of the Academy of Finland for financial support.

[1]R. Dörner, V. Mergel, O. Jagutzki, L. Speilberger, J. Ullrich, R. Moshammer, and H. Schmidt-Böcking, Phys. Rep. **330**, 95 (2000).
[2]J. Ullrich, R. Moshammer, A. Dorn, R. Dörner, L. P. H. Schmidt, and H. Schmidt-Böcking, Rep. Prog. Phys. **66**, 1463 (2003).
[3]N. Neumann, D. Hant, L. P. H. Schmidt, J. Titze, T. Jahnke, A. Czasch, M. S. Schöffler, K. Kreidi, O. Jagutzki, H. Schmidt-Böcking, and R. Dörner, Phys. Rev. Lett. **104**, 103201 (2010).
[4]C. Miron and P. Morin, *Handbook of High-Resolution Spectroscopy*, edited by M. Quack and F. Merkt (Wiley, Chichester, U.K., 2011), p. 1655
[5]D. Céolin, C. Miron, M. Simon, and P. Morin, J. Electron Spectrosc. Relat. Phenom. **141**, 171 (2004).
[6]G. R. Wight and C. E. Brion, J. Electron Spectrosc. Relat. Phenom. **3**, 191 (1974).
[7]W. D. H. Köppel and L. S. Cederbaum, Adv. Chem. Phys. **57**, 59 (1984).
[8]K. Ueda and J. H. D. Eland, J. Phys. B: At. Mol. Opt. Phys. **38**, 839 (2005).
[9]Y. Muramatsu, K. Ueda, N. Saito, H. Chiba, M. Lavolée, A. Czasch, T. Weber, O. Jagutzki, H. Schmidt-Böcking, R. Moshammer, U. Beckerand, K. Kubozuka, and I. Koyano, Phys. Rev. Lett. **88**, 133002 (2002).
[10]S. Miyabe, C. W. McCurdy, A. E. Orel, and T. N. Rescigno, Phys. Rev. A **79**, 053401 (2009).
[11]N. Saito, K. Ueda, A. D. Fanis, K. Kubozuka, M. Machida, I. Koyano, R. Dörner, A. Czasch, L. Schmidt, A. Cassimi, K. Wang, B. Zimmermann, and V. McKoy, J. Phys. B **38**, L277 (2005).
[12]M. Ehara and K. Ueda, J. Phys.: Conf. Ser. **235**, 012020 (2010).
[13]J. Adachi, N. Kosugi, E. Shigemasa, and A. Yagishita, J. Chem. Phys. **107**, 4919 (1997).
[14]P. Morin, M. Simon, C. Miron, N. Leclercq, E. Kukk, J. Bozek, and N. Berrah, Phys. Rev. A **61**, 050701 (2000).
[15]G. Öhrwall, M. M. S. Anna, W. C. Stolte, I. Dominguez-Lopez, L. T. N. Dang, A. S. Schlachter, and D. W. Lindle, J. Phys. B: At. Mol. Opt. Phys. **35**, 4543 (2002).
[16]T. Masuoka, J. Electron Spectrosc. Relat. Phenom. **101**, 53 (1999).
[17]J. D. Bozek, N. Saito, and I. H. Suzuki, Phys. Rev. A **51**, 4563 (1995).
[18]R. K. Kushawaha, S. S. Kumar, I. A. P. K. P. Subramanian, and B. Bapat, J. Phys. B **42**, 105201 (2009).
[19]M. Alagia, P. Candori, S. Falcinelli, F. P. M. Lavollée, R. Richter, S. Stranges, and F. Vecchiocattivi, J. Phys. Chem. A **113**, 14755 (2009).
[20]B. Bapat and V. Sharma, J. Phys. B: At. Mol. Opt. Phys. **40**, 13 (2007).
[21]J. H. D. Eland, L. Andric, P. Linusson, L. Hedin, S. Plogmaker, J. Paladoux, F. Penent, P. Lablanquie, and R. Feifel, J. Phys. Chem. **135**, 134309 (2011).
[22]C. Tian and C. R. Vidal, Phys. Rev. A **58**, 3783 (1998).
[23]T. Masuoka, Phys. Rev. A **50**, 3886 (1994).
[24]M. Hochlaf, F. R. Bennett, G. Chambaud, and P. Rosmus, J. Phys. B: At. Mol. Opt. Phys. **31**, 2163 (1998).
[25]M. Alagia, P. Candori, S. Falcinelli, M. Lavollé, F. Pirani, R. Richter, S. Stranges, and F. Vecchiocattivi, Phys. Chem. Chem. Phys. **12**, 5389 (2010).
[26]T. Masuoka, E. Nakamura, and A. Hiraya, J. Chem. Phys. **104**, 6200 (1996).
[27]L. Journel, R. Guillemin, A. Haouas, F. P. P. Lablanquie, L. A. J. Palaudoux, M. Simon, D. Ceolin, T. Kaneyasu, J. Viefhaus, W. B. L. M. Braune, F. C. C. Elkharrat, J.-C. Houver, and D. Dowek, Phys. Rev. A **77**, 042710 (2008).
[28]J. Laksman, D. Céolin, M. Gisselbrecht, and S. L. Sorensen, "Development and characterization of a multiple coincidence ion momentum imaging spectrometer," Rev. Sci. Instrum. (unpublished).
[29]M. Bässler, A. Ausmees, M. Jurvansuu, R. Feifel, J.-O. Forsell, P. de TarsoFonseca, A. Kivimäki, S. Sundin, S. L. Sorensen, R. Nyholm, O. Björneholm, S. Aksela, and S. Svensson, Nucl. Instrum. Methods **469**, 382 (2001).
[30]R. N. Zare, Mol. Photochem. **4**, 1 (1972).
[31]N. Saito and K. Ueda, Phys. Rev. A **62**, 052503 (2000).
[32]A. I. Chichinin, T. S. Einfeld, K. H. Gericke, and C. Maul, *Imaging in Molecular Dynamics*, edited by E. B. Whitaker (Cambridge University Press, Cambridge, 2003), p. 153
[33]T. Tanaka, C. Makochekanwa, H. Tanaka, M. Kitajima, M. Hoshino, Y. Tamenori, G. P. E. Kukk, X. J. Liu, and K. Ueda, Phys. Rev. Lett. **95**, 203002 (2005).
[34]H. Yoshida, K. Nobusada, K. Okada, S. Tanimoto, N. Saito, A. D. Fanis, and K. Ueda, Phys. Rev. Lett. **88**, 083001 (2002).
[35]J. Laksman, D. Céolin, M. Gisselbrecht, S. E. Canton, and S. L. Sorensen, J. Chem. Phys. **131**, 244305 (2009).
[36]J. Laksman, D. Céolin, M. Gisselbrecht, and S. L. Sorensen, J. Chem. Phys. **133**, 144314 (2010).
[37]Z. D. Pešič, D. Rolles, R. C. Bilodeau, I. Dimitriu, and N. Berrah, Phys. Rev. A **78**, 051401 (2008).
[38]R. H. Dalitz, Philos. Mag. **44**, 1068 (1953).
[39]C. Maul and K. H. Gericke, J. Phys. Chem. A **104**, 2531 (2000).